Available online at www.sciencedirect.com
SCIENCE DIRECT®
Journal of Solid State Chemistry 179 (2006) 2141–2149
JOURNAL OF SOLID STATE CHEMISTRY
www.elsevier.com/locate/jssc

Crystal chemistry on a lattice: The case of BZN and BZN-related pyrochlores

Yun Liu[a], Ray L. Withers[a,*], T.R. Welberry[a], Hong Wang[b], Huiling Du[b]

[a]*Research School of Chemistry, Australian National University, Canberra, A.C.T 0200, Australia*
[b]*Electronic Materials Research Laboratory, Xian Jiaotong University, Xian, Shaanxi 710049, PR China*

Received 3 March 2006; received in revised form 13 April 2006; accepted 16 April 2006
Available online 25 April 2006

Abstract

This paper uses a diagnostic, highly structured diffuse intensity distribution to investigate the local crystal chemistry of $(Bi_{1.5}Zn_{0.5-\delta})(Zn_{0.5}Nb_{1.5})O_{7-\delta}$ (BZN) as well as Sn^{4+} and Ti^{4+}, *B* site substituted, BZN-related pyrochlore phases. The structured diffuse distribution of the *B* site substituted material is found to be remarkably similar to that observed for BZN itself. In the special case of $(Bi_{1.5}Zn_{0.5})(Ti_{1.5}Nb_{0.5})O_7$ (BZNT), the continuous $\mathbf{G}\pm\langle 10l\rangle^*$ type diffuse streaking characteristic of BZN-related pyrochlores has virtually condensed out to give just $\mathbf{G}\pm\langle 001\rangle^*$ "satellite reflections" and a *P*-centred, close to a superstructure phase of average pyrochlore unit cell dimensions. Bond valence sum considerations are used to investigate the local crystal chemistry of this BZNT phase and to derive a plausible model for this superstructure phase. Monte Carlo modelling is used to confirm the plausibility of the model proposed. The underlying crystal chemistry of BZN and BZN-related pyrochlores is shown to result from strong local Bi/Zn ordering rules and associated large amplitude structural relaxation.

Keywords: BZN-related pyrochlores; Structured diffuse distribution; Superstructure phase; Crystal chemistry; Zincanyl structural units; Electron diffraction study

1. Introduction

The *A* and *B* site 'disordered' cubic pyrochlore $(Bi_{1.5}Zn_{0.5-\delta})(Zn_{0.5}Nb_{1.5})O_{7-\delta}$ (BZN) is an attractive candidate material for future wireless communications technology as a result of its high (as well as tuneable) dielectric constant and low dielectric loss in the RF/microwave frequency range coupled with its relatively low sintering temperature. Its structure and physical properties have thus been intensively investigated over recent times [1–8].

The realization that BZN is but one of a large and rapidly growing family of inherently disordered cubic $A_2B_2O_7$ pyrochlores, all characterized by extensive displacive disorder apparently induced by the presence of nominally too small cations such as Zn^{2+}, Cu^{2+}, Mg^{2+}, Mn^{2+} or Ni^{2+} occupying ~25% of the large *A* cation sites of the ideal pyrochlore structure type (see Fig. 1), raises intriguing questions as to the fundamental underlying crystal chemistry of such materials [8–12]. In addition, the extraordinary compositional flexibility of this family of materials is also of practical interest in that the wide range of substitutions allowed on both the *A* and *B* sites enables the associated dielectric properties to be systematically altered and thus potentially tuned ([9–10,13–15]; see also Table 1). Not only can the Zn^{2+} in BZN be replaced with other 2+ ions such as e.g., Cu, Mg, Mn or Ni, but individual substitutions of both *A* as well as *B* site cations can also be made. The associated dielectric properties of some BZN-related materials have been shown to be considerably affected by such substitutions [13–15] (Table 1).

The focus of the current paper is on the *B* site substituted $(Bi^{3+}_{1.5}Zn^{2+}_{0.5})$ $(Zn^{2+}_{0.5-x/3}Ti^{4+}_{x}Nb^{5+}_{1.5-2x/3})O_7$ and $(Bi^{3+}_{1.5}Zn^{2+}_{0.5})$ $(Zn^{2+}_{0.5-x/3}Sn^{4+}_{x}Nb^{5+}_{1.5-2x/3})O_7$, $0\leqslant x\leqslant 1.5$, BZN-related solid solutions [13,14] and, in particular, on the effect that such

*Corresponding author. Fax: +61 2 6125 0750.
E-mail address: withers@rsc.anu.edu.au (R.L. Withers).

0022-4596/$ - see front matter © 2006 Elsevier Inc. All rights reserved.
doi:10.1016/j.jssc.2006.04.017

B site substitutions have upon Bi/Zn and/or Zn/Nb ordering and associated structural relaxation. Such disorder has recently been shown to be responsible for a highly structured diffuse intensity distribution in the case of BZN itself [8]. Furthermore, this characteristic diffuse distribution has been shown to arise primarily from Bi/Zn ordering on the pyrochlore *A* sites coupled with associated large amplitude displacive relaxation of the atoms occupying the O′ and *A* sites [8]. Given that extensive displacive disorder on the O′ and *A* sites has been linked to both the high dielectric constant as well as the anomalous and deleterious low temperature glass-like dielectric relaxation behaviour of BZN [5,6], it is clearly of importance to understand its crystal chemical origin as well as the effect of doping upon it.

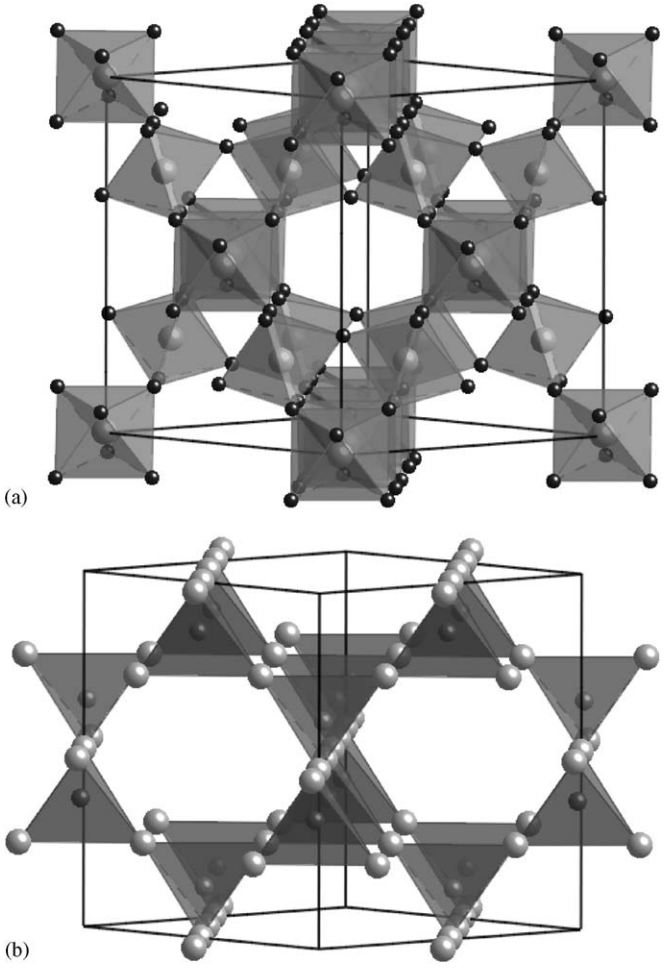

Fig. 1. Shows the two intergrown component sub-structures of the ideal cubic pyrochlore structure type. The first (a) is a B_2O_6 array of corner-connected, cation-centred BO_6 octahedra while the second (b) is an $O'A_2$ array of corner-connected, oxygen-centred tetrahedra (of ideal anti-β-cristobalite structure type).

2. Experimental

(Bi1.5Zn0.5) $(Zn_{0.5-x/3}Ti_xNb_{1.5-2x/3})O_7$ (BZTN), $x = 0.0$, 0.25, 0.5, 1.0 and 1.5 and $(Bi_{1.5}Zn_{0.5})(Zn_{0.5-x/3}Sn_xNb_{1.5-2x/3})O_7$ (BZSN), $x = 0.0$, 0.25, 0.5, 1.0 and 1.5 samples were synthesized by conventional solid state reaction using high purity Bi_2O_3, ZnO, Nb_2O_5, SnO_2 and TiO_2 oxide starting materials. For the BZTN samples, the raw materials were homogeneously mixed for 4 h using an agate ball mill of planetary type and then calcined at 700–800 °C for 2 h. The resultant powders were then re-ground and pressed into pellets. Finally, the pellets were annealed from 960 to 1100 °C for 2 h in air and then furnace-cooled. For the BZSN samples, the same process was followed except that the final annealing temperature was slightly higher than that for BZTN, from 1100 to 1200 °C. In general, the higher the Ti (or Sn) content, the higher the required annealing temperature. The detailed synthesis routes and processing parameters used are described in Refs. [13–15].

Powder XRD data of these samples was collected using a Guinier–Hägg camera and Cu$K\alpha_1$ radiation. Si (NBS #640c, $a = 5.431195(9)$ Å at 22.5 °C) was used as an internal standard in order to accurately determine unit cell parameters. Samples suitable for transmission electron microscopy (TEM) were prepared by the dispersion of finely ground material onto a holey carbon film. Electron

Table 1
Reported dielectric properties of *A* and *B* site doped BZN-related ceramics

Composition	Dielectric constant ε	Dielectric loss tg δ	TCC (ppm/°C)	Ref.
$(Bi_{1.5}Zn_{0.4}Cd_{0.1})(Sb_{1.5}Zn_{0.5})O_7$	33.4@100 kHz	0.002	—	[10]
$(Bi_{1.5}Zn_{0.3}Cd_{0.2})(Sb_{1.5}Zn_{0.5})O_7$	34.8@100 kHz	0.0025	—	[10]
$(Bi_{1.5}Zn_{0.4}Sr_{0.1})(Sb_{1.5}Zn_{0.5})O_7$	33.9@100 kHz	0.001	—	[10]
$(Bi_{1.5}Zn_{0.4}Ca_{0.1})(Sb_{1.5}Zn_{0.5})O_7$	31.9@100 kHz	0.0046	—	[10]
$(Bi_{1.5}Zn_{0.5})(Nb_{1.5}Zn_{0.5})O_7$	152@1 MHz	0.0003	−470	[3]
$(Bi_{1.3}Gd_{0.2}Zn_{0.5})(Nb_{1.5}Zn_{0.5})O_7$	116@1 MHz	0.0004	−350	[3]
$(Bi_{1.5}Zn_{0.5})(Nb_{0.5}Ti_{1.5})O_7$	200@1 MHz	0.0001	−1300	[3]
$(Bi_{1.3}Gd_{0.2}Zn_{0.5})(Nb_{0.5}Ti_{1.5})O_7$	143@1 MHz	0.0006	−560	[3]
$(Bi_{1.5}Zn_{0.5})(Ta_{1.5}Zn_{0.5})O_7$	76@1 MHz	0.0001	−146	[15]
$(Bi_{1.5}Zn_{0.5})(Sb_{1.5}Zn_{0.5})O_7$	32@1 MHz	0.0001	−98	[15]
$Bi_2(Zn_{2/3}Nb_{4/3})O_7$	90@1 MHz	0.0007	+150	[3]
$(Bi_{1.8}Gd_{0.2})(Zn_{2/3}Nb_{4/3})O_7$	80@1 MHz	0.0005	+240	[3]

TCC = temperature coefficient of capacitance.

diffraction patterns (EDPs) were obtained using a Philips EM 430 TEM.

3. Results

3.1. XRD results

Each of the samples were single phase and of cubic pyrochlore average structure type. Fig. 2 shows the observed variation in the refined cubic lattice parameter as a function of composition for both the BZSN and BZTN samples. On the basis of ionic size considerations [16], one might expect that the replacement of ($\frac{1}{3}$ Zn^{2+} + $\frac{2}{3}$ Nb^{5+}) (of average ionic radius 0.81 Å) with one slightly larger Sn^{4+} ion (of ionic radius ~0.83 Å) should lead to a small but systematic expansion in the average cubic pyrochlore unit cell dimension which indeed it does — from 10.5465 Å at $x = 0$ up to 10.5895 Å at $x = 1.5$. On the other hand, the replacement of ($\frac{1}{3}$ Zn^{2+} + $\frac{2}{3}$ Nb^{5+}) with a signicantly smaller Ti^{4+} ion (of ionic radius ~0.745 Å) leads to a systematic and rather faster reduction in the cubic pyrochlore unit cell dimension from 10.5465 Å at $y = 0$ down to 10.351 Å at $x = 1.5$. The question is: what effect do such lattice parameter changes, *B* site substitutions and associated displacive relaxations have upon the Bi/Zn ordering and associated structural relaxation characteristic of the O′A_2 sub-structure (see Fig. 1b)?

3.2. Electron diffraction results

In general, the BZSN and BZTN samples exhibit very similar structured diffuse intensity distributions to that characteristic of BZN itself, showing that *B* site ordering and associated structural relaxation has remarkably little influence upon the compositional and displacive disorder

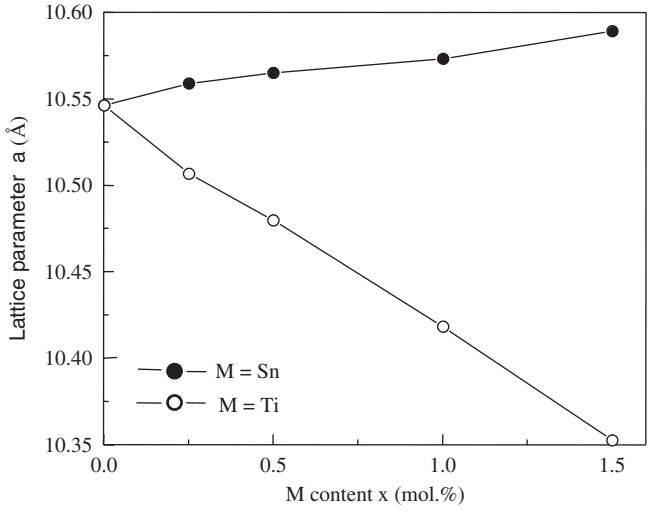

Fig. 2. The refined cubic lattice parameter of the underlying pyrochlore type average structure as a function of composition for both the BZSN and BZTN samples.

associated with the O′A_2 sub-structure. Fig. 3a, for example, shows a ⟨118⟩ zone axis EDP typical of BZN obtained by tilting ~10° away from the ⟨001⟩ zone axis orientation keeping the $[2\bar{2}0]^*$ systematic row excited. Fig. 3c shows the equivalent, and virtually identical, ⟨118⟩ zone axis EDP of BZSN, $x = 1.0$. Likewise, Fig. 3b shows a typical ~⟨551⟩ zone axis EDP of BZN obtained by tilting ~9° away from a ⟨110⟩ zone axis orientation again keeping a $[2\bar{2}0]^*$ systematic row excited. Fig. 3d shows the equivalent, and again similar, ~⟨551⟩ zone axis EDP of BZTN, $x = 1.5$.

For comparison purposes, Figs. 3e and f show the equivalent ⟨118⟩ and ⟨551⟩ zone axis EDPs obtained via Monte Carlo simulation of the O′$Bi_{1.5}Zn_{0.5}$ sub-structure of BZN (using the relaxed $\frac{2}{3}$ E_1 + $\frac{1}{3}$ E_2 distribution; see [8] for the details). As described in [8], E_1 is minimized when all O′A_4 tetrahedra have stoichiometry O′Bi_3Zn while E_2 is minimized when $\frac{1}{2}$ ⟨110⟩ type Zn–Zn separation distances are completely avoided. The clearly close agreement between the simulated and experimental EDP's suggests that the same local chemical ordering principles occur in both BZSN and BZTN as well as BZN itself.

Note the existence of strong blobs of diffuse intensity (virtual "satellite reflections") at the **G**±~⟨001⟩* (**G** a pyrochlore average structure Bragg reflection) positions of reciprocal space (e.g., at $[44\bar{1}]^*$ in (a) and (c)) along with characteristic diffuse streaking running through these blobs along the ⟨100⟩* and ⟨010⟩* reciprocal space directions. The limited extent of the diffuse streaking along the $[80\bar{1}]^*$ and $[08\bar{1}]^*$ directions of reciprocal space in Figs. 3a and c arises from the fact that the [100]* and [010]* directions of reciprocal space lie slightly out of the plane at this ⟨118⟩ zone axis orientation. This is confirmed by the (a) close to ⟨110⟩ and (b) $\langle\bar{1}\bar{1}6\rangle$ zone axis EDP's of the BZSN, $x = 1.0$, sample shown in Fig. 4. Very similar EDP's have been obtained for all BZSN samples. Clearly, strong diffuse intensity still occurs at the **G**±[10*l*]*, **G**±[1*k*0]*, **G**±[*h*10]*, **G**±[01*l*]*, **G**±[10*l*]*, **G**±[*h*01]* and **G**±[*h*10]* (*h*,*k*,*l* continuous; hereafter labelled **G**± ⟨10*l*⟩*) positions of reciprocal space, exactly as found for BZN itself (see [8]). Equally clearly, the Bi/Zn ordering and associated structural relaxation responsible is still very much present in the case of the *B* site substituted samples [8].

In the case of the BZTN samples, similar behaviour is in general again observed except for the high *x*, $x = 1.5$, sample, $(Bi^{3+}_{1.5}Zn^{2+}_{0.5})(Ti^{4+}_{1.5}Nb^{5+}_{0.5})O_7$, where the extended diffuse streaks in the case of the other samples have noticeably shrunk in extent such that the diffuse distribution appears to be very close to condensing out at the **G**±⟨001⟩* positions of reciprocal space—giving rise to what would appear to be a *P*-centred resultant superstructure of average pyrochlore unit cell dimensions. This is already apparent in Fig. 3d but is even more apparent in the (a) [001] and (b) ⟨221⟩ zone axis EDPs of the $x = 1.5$ BZTN sample shown in Fig. 5. The 'reflection' labelled

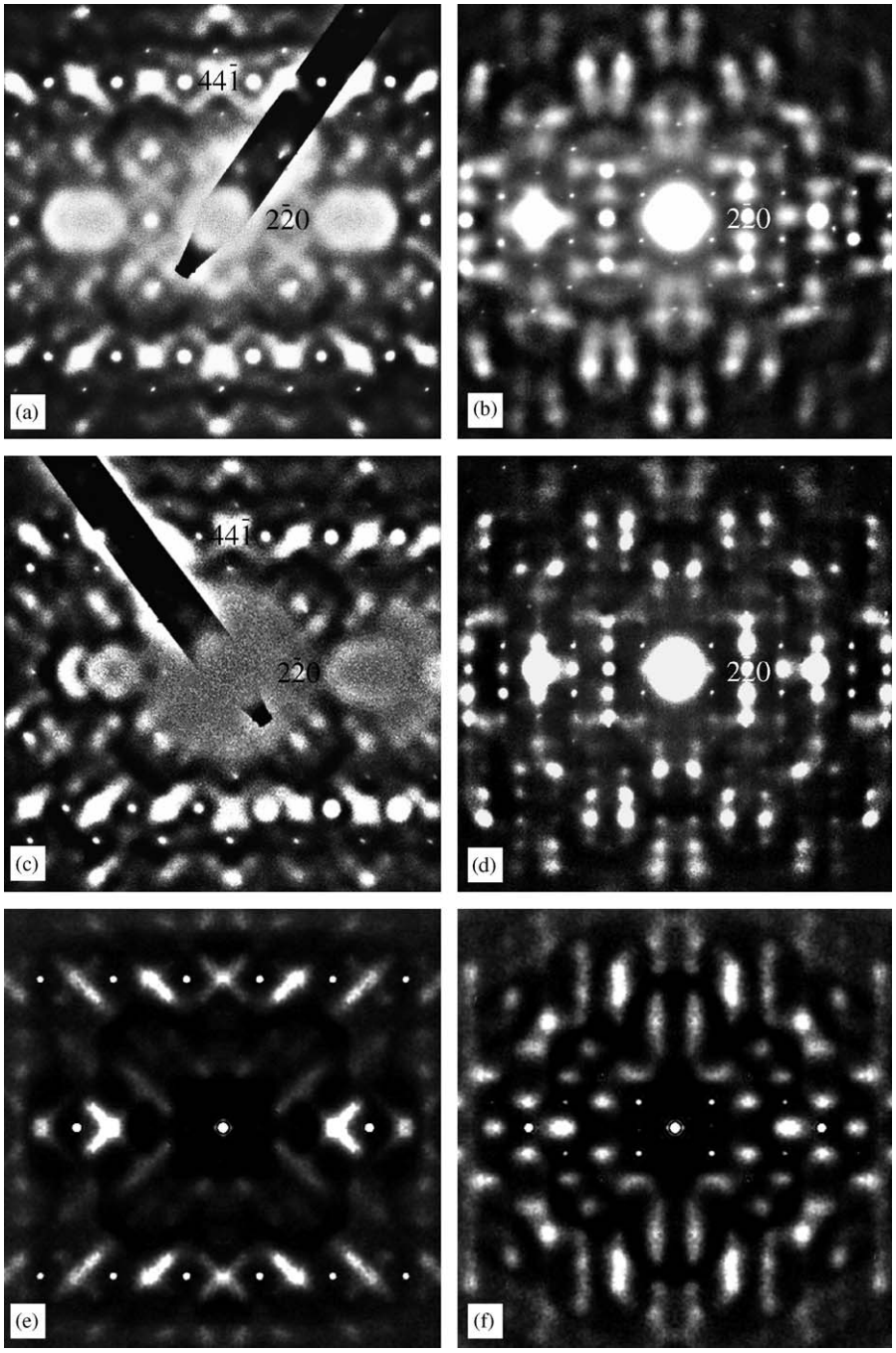

Fig. 3. $\langle 118 \rangle$ zone axis EDPs typical of (a) BZN and (c) BZSN, $x = 1.0$, obtained by tilting $\sim 10^{\circ}$ away from the $\langle 001 \rangle$ zone axis orientation keeping a $[22\bar{0}]^{*}$ systematic row excited. Also $\langle 551 \rangle$ zone axis EDP's of (b) BZN and (d) BZTN, $x = 1.5$, obtained by tilting $\sim 9^{\circ}$ away from a $\langle 110 \rangle$ zone axis orientation again keeping a $[22\bar{0}]^{*}$ systematic row excited. Note the presence of strong blobs of diffuse intensity ("satellite reflections") at the $\mathbf{G} \pm \sim \langle 001 \rangle^{*}$ positions of reciprocal space (e.g. at $[44\bar{1}]^{*}$ in (a) and (c)) along with the presence of diffuse streaking running through and connecting these diffuse blobs of intensity along the $\langle 100 \rangle^{*}$ and $\langle 010 \rangle^{*}$ directions of reciprocal space. For comparison purposes, Figs. 3e and f show the equivalent $\langle 118 \rangle$ and $\langle 551 \rangle$ zone axis EDPs obtained via Monte Carlo simulation of the $O'Bi_{1.5}Zn_{0.5}$ sub-structure of BZN.

[102]* in Fig. 5b, for example, is not an allowed Bragg reflection of the $Fd\bar{3}m$ average pyrochlore structure type.

Clearly, there is a much greater tendency towards long range ordering in the case of $(Bi^{3+}_{1.5}Zn^{2+}_{0.5})(Ti^{4+}_{1.5}Nb^{5+}_{0.5})O_7$. This 'very close to a superstructure' state is intriguing from the point of view of understanding the fundamental crystal chemistry of BZN-related pyrochlores in that it is rather easier to model and understand than the more disordered BZN itself. For the remainder of this paper, the focus is therefore on this BZTN, $x = 1.5$ sample.

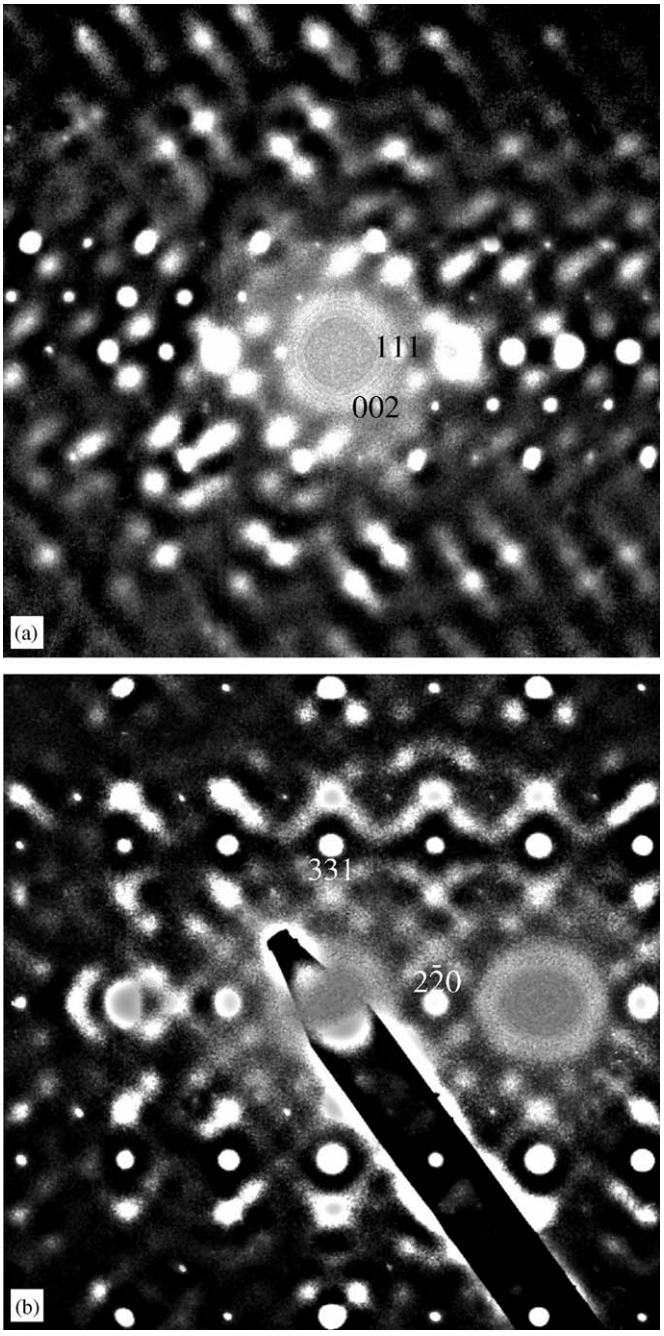

Fig. 4. (a) Close to ⟨110⟩ and (b) [1$\bar{1}$6] zone axis EDPs typical of BZSN, $x = 1.0$.

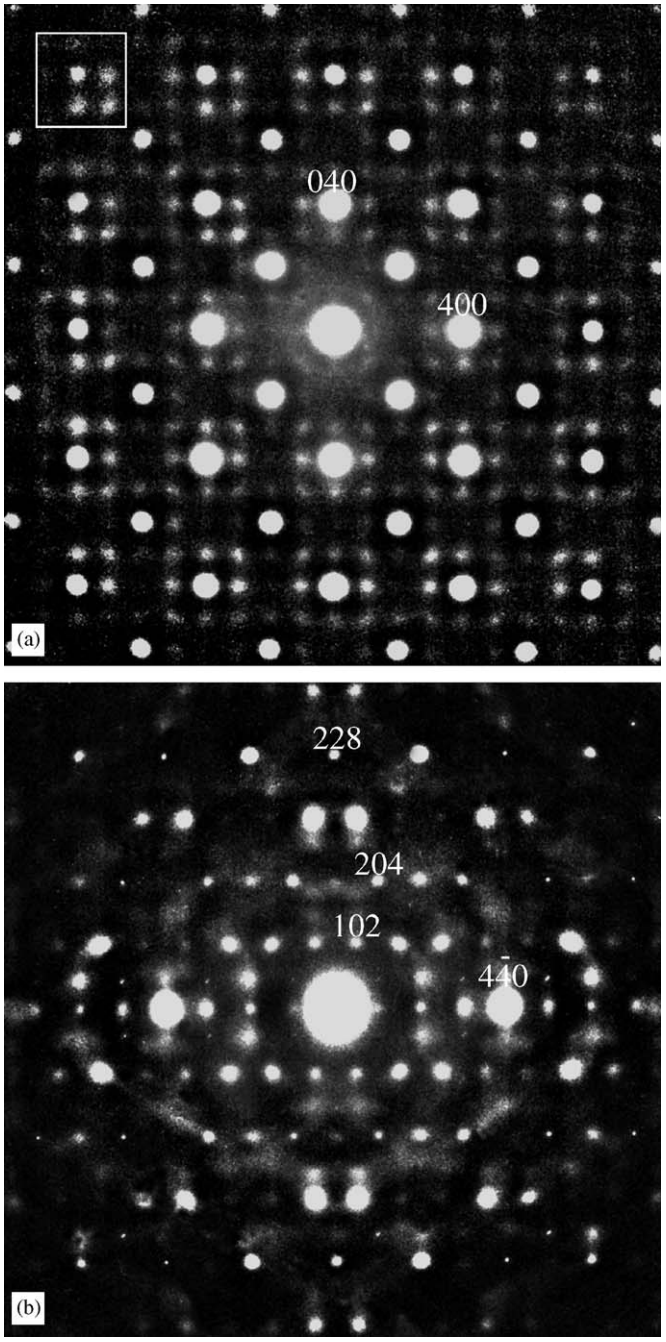

Fig. 5. (a) [001] and (b) ⟨221⟩ zone axis EDPs typical of the BZTN, $x = 1.5$, sample. The strong blobs of diffuse intensity ("satellite reflections") at the $\mathbf{G} \pm \sim \langle 001 \rangle^*$ positions of reciprocal space (e.g. the reflection labelled [102]* in Fig. 5b) are clearly still present. The extended diffuse streaking through these satellite reflections along the $\langle 001 \rangle^*$ directions of reciprocal space typical of BZN and BZSN (cf. e.g. with Fig. 4), however, have vanished.

4. Crystal chemistry of BZTN and BZN-related pyrochlores

4.1. The average structure

The $A_2B_2O_7$ cubic average structure type (see Fig. 1) of $(Bi_{1.5}Zn_{0.5})$ $(Nb_{0.5}Ti_{1.5})O_6O'_1$ (BZTN) has space group symmetry $Fd\bar{3}m$, with A on 16d at $\frac{1}{2}, \frac{1}{2}, \frac{1}{2}$; B on 16c at 0, 0, 0; O on 48f at $x, \frac{1}{8}, \frac{1}{8}$; and O′ on 8$b$ at $\frac{3}{8}, \frac{3}{8}, \frac{3}{8}$. It can be described in terms of a B_2O_6 octahedral corner-connected sub-structure (see Fig. 1a) intergrown with an $O'A_2$ tetrahedral corner-connected sub-structure of anti-cristobalite structure type (see Fig. 1b). The two sub-structures are not independent, however, as the A cations of the latter are bonded reasonably strongly to the O anions of the former, particularly when $A = Bi$. Breaking the ideal cubic pyrochlore structure type up in this way is nonetheless a very

useful way to investigate the crystal chemistry of the overall structure (see e.g. [8]).

4.1.1. The B_2O_6 octahedral sub-structure

Consider firstly the B_2O_6 octahedral corner-connected sub-structure (see Fig. 1a). The B cations in this sub-structure are octahedrally co-ordinated by 6 O ions at an average distance $R(B\text{–O}) = \sqrt{\{(x-1/4)^2 + 2(1/8)^2\}} \times 10.3528$ Å which is dependant on the one unknown fractional co-ordinate of the ideal pyrochlore structure type, the x co-ordinate of the O ion, as well as the cubic lattice parameter a (= 10.3528 Å in the case of BZNT).

For Nb^{5+} in the B site, the ideal B–O distance R(Nb–O) is given by that distance which corresponds to an apparent valence (AV) (see [17]) of $\frac{5}{6}$. From [17], this distance is given by $1.911-0.37\ln(5/6) = 1.9785$ Å. For Ti^{4+} in the same B site, the equivalent ideal B–O distance R(Ti–O) = $1.815-0.37\ln(4/6) = 1.9650$ Å again using the R_0 parameters listed in [17]. Note that these two ideal bond lengths are very close to one another and much closer than they are either in the case of BZN (see [8]) or e.g. BZSN where the ideal B–O distance $R(Sn^{4+}\text{–O}) = 1.905-0.37\ln(4/6) = 2.0550$ Å as compared to the ideal R(Nb–O) of 1.9785 Å. Thus, only very small relaxations of the O array associated with the local distribution of Nb^{5+} and Ti^{4+} on the B site positions is necessary in the case of BZTN.

Given that the average occupancy of the B site is $\frac{3}{4}$ Ti + $\frac{1}{4}$Nb, the expected average B–O bond length, $R(B\text{–O})$ should be such that $AV(B) = 6 \times 1/4 \times \exp\{(1.911-R)/0.37\}1 + 63/4 \times \exp\{(1.815-R)/0.37\} = 1/4 \times 5 + 3/4 \times 4 = 4.25$. This occurs for $R = 1.9690$ Å. An average $R(B\text{–O})$ bond length of 1.9690 Å occurs for $x = 0.3202$ given the relation between $R(B\text{–O}) = \sqrt{\{(x-1/4)^2 + 2(1/8)^2\}} \times 10.3528$ Å and x. The bond valence sum prediction for the value of x is thus 0.3202 in the case of BZTN. Given such a value for x, the 'average' B cation will then be happily bonded in the average pyrochlore structure, as is clear from the bond valence sums, or AVs, calculated for BZNT assuming $x = 0.3202$ and $a = 10.3528$ Å (see Table 2). Table 3 then shows the calculated AV of the O′ ion depending upon the local [A_4] stoichiometry while Table 4 shows the calculated AV of the O ion dependant upon its local [A_2B_2] stoichiometry.

Table 2
Bond valence sums (AVs) for the cubic pyrochlore average structure assuming $x = 0.3202$, $a = 10.3528$ Å

A	B	AV(A)	AV(B)	AV(O)	AV(O′)
Bi	Nb	2.828	5.129	2.205	2.685
Bi	Ti	2.828	3.957	1.814	2.685
Zn	Nb	0.985	5.129	1.882	0.936
Zn	Ti	0.985	3.957	1.491	0.936

Table 3
AVs for O' dependent upon local [A_4] stoichiometry

	[Bi_4]	[Bi_3Zn]	[Bi_2Zn_2]	[$BiZn_3$]	[Zn_4]
AV(O′)[A_4]	2.685	2.2478	1.811	1.373	0.936

Table 4
AVs for O dependent upon local [A_2B_2] stoichiometry

	[Bi_2Ti_2]	[Bi_2TiNb]	[$BiZnTi_2$]	[BiZnTiNb]
AV(O)[A_2B_2]	1.814	1.638	2.009	1.848

4.1.2. The $O'A_2$ anti-cristobalite tetrahedral sub-structure

Now consider the second $O'A_2$ tetrahedral corner-connected substructure of anti-cristobalite structure type (see Fig. 1c). The O′ anion in this average sub-structure is tetrahedrally co-ordinated by 4 A cations at an average distance $R(O'\text{–}A) = (\sqrt{3}/8)a = 2.2414$ Å determined solely by the cubic lattice parameter a. The ideal O′–A distance, R(O′–Bi), for an $O'Bi_4$ tetrahedron is given by that distance which corresponds to an AV of $\frac{2}{4}$. From [17], this distance is given by $2.094\text{–}0.37\ln 2/4 = 2.3505$ Å. The equivalent ideal O′–A distance, R(O′–Zn), for an $O'Zn_4$ tetrahedron is given by $R(O'\text{–Zn}) = 1.704\text{–}0.37\ln 2/4 = 1.9605$ Å. Note that these two ideal bond lengths this time differ quite significantly from each other and from the average O′–A distance of 2.2414 Å. Substantial strain relaxation of the $O'A_2$ array can thus be expected associated with the local distribution of Bi^{3+} and Zn^{2+} on the A sites of the average pyrochlore structure, as is characteristic of all BZN-related pyrochlores. Table 3 shows the calculated AV of the O′ ion depending upon the local [A_4] stoichiometry. It can readily be seen that by far the most likely local tetrahedral stoichiometry is O′[Bi_3Zn]. While O′[Bi_2Zn_2] also appears possible from Table 3, bear in mind that the average stoichiometry necessitates that for every $O'Bi_2Zn_2$ tetrahedron there must necessarily exist a strongly unfavourable, balancing $O'Bi_4$ tetrahedron. There is thus a strong driving force for each local $O'A_4$ tetrahedron to have the average stoichiometry i.e. O′[Bi_3Zn].

4.1.3. Inter-substructure interactions

Attention so far has focussed on satisfying the bond valence sum requirements of the B and O′ ions. What about the A and O ions? The A cation in the pyrochlore average structure type is in an essentially hexagonal prismatic site surrounded by 6 equatorial O ions and 2 apical O′ ions (see Fig. 6) and is always under-bonded, desperately so when Zn^{2+} occupies the site (AV = 0.985 instead of 2.0 valence units (v.u's), see Table 2). Given the weakness of the bonding between the central Zn ion and each of the six surrounding equatorial O ions (~0.086 v.u′s), the only way in which this massive under-bonding can be remedied on the local scale is for the two O′ anions

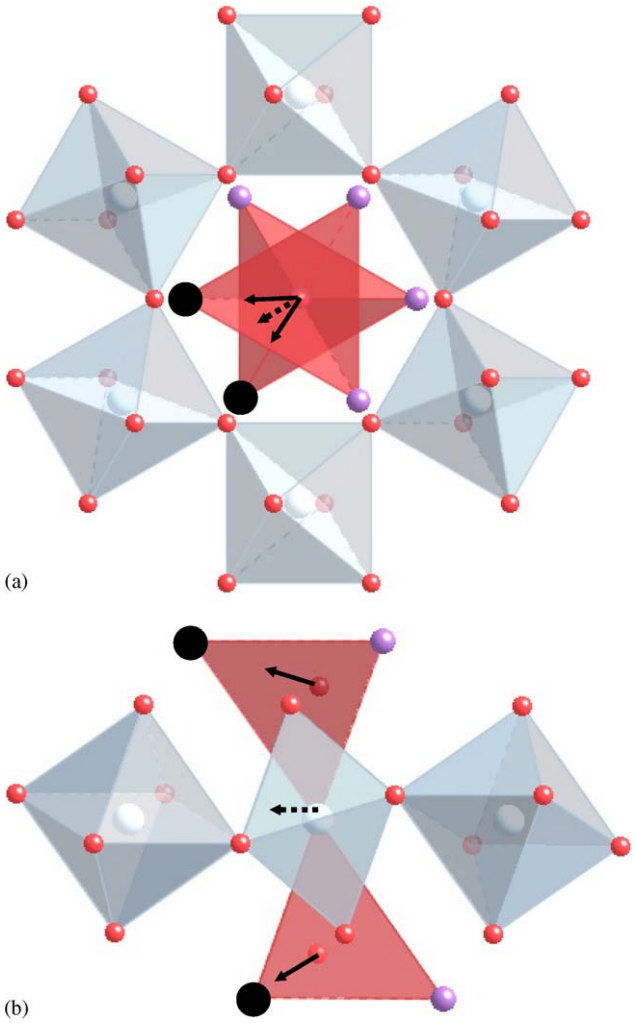

Fig. 6. Shows the essentially hexagonal prismatic environment of the A cations in the pyrochlore average structure type, in projection along $\langle 111 \rangle$ in (a) and along $\langle 1\bar{1}0 \rangle$ in (b). The largest black spheres represent Zn ions, the medium lighter spheres represent Bi ions and the smallest spheres represent O ions. The displacements of the O′ ions (initially centreing the two O′Bi_3Zn tetrahedra shown) towards the Zn ions in each tetrahedra are shown by the solid lines while the induced shift of the central Bi ion $\mathbf{u}_{Bi} = \frac{1}{2}(\mathbf{u}_{O1'} + \mathbf{u}_{O2'})$ is represented by the dashed line. Note that the central Bi ion thus moves off-centre towards two of the 6 surrounding equatorial O ions whilst simultaneously minimizing the separation distance to its two surrounding apical O′ ions.

on either side of a central Zn^{2+} ion to simultaneously contract in towards it along a local $\langle 111 \rangle$ direction. A coupled contraction of this sort goes a long way towards the formation of a local ZnO'_2 "zincanyl" type unit. A simultaneous reduction in the two apical Zn–O′ distances from 2.2414 to 1.8147 Å, for example, raises the AV of the central Zn ion all the way up from 0.985 to the desired 2.0 v.u's [17]. Such O′ shifts, however, without a simultaneous coupled relaxation of the surrounding Bi ions, also necessarily expand the remaining 3 O′–Bi distances (from the initial 2.2414–2.4174 Å). This in turn leads to a significant reduction in the bond valence sum contributions of the 2 O′ ions bonded to each Bi ion and to severely under-bonded Bi ions (AV of 2.320 instead of the initial 2.828).

The only means to improve the now significant under-bonding of the Bi^{3+} ions is for them to move off-centre towards one or more of the 6 surrounding equatorial O ions whilst simultaneously minimizing the separation distance to their two surrounding apical O′ ions. This latter condition is equivalent to the requirement that $\mathbf{u}_{Bi} = \frac{1}{2}(\mathbf{u}_{O1'} + \mathbf{u}_{O2'})$ i.e. the local shift of the Bi ion is determined by the shifts of the two O′ ions to which it is bonded. In turn, these O′ shifts are determined by the local distribution of Zn ions within each O′Bi_3Zn tetrahedron (see e.g. Fig. 6).

Given a starting Zn ion and assuming that each tetrahedron has the ideal O′Bi_3Zn stoichiometry, there are only two possible types of inter-tetrahedral Zn–Zn separation distances. The first is of $\frac{1}{4}\langle 112 \rangle$ type as shown in Fig. 6 and automatically induces shifts of the Bi ions perpendicular to the local O′–Bi–O′ axis towards two of the six surrounding equatorial O ions as required both from the crystal chemical and average structure refinement [6,8] points of view. The second, and only other, possible type of inter-tetrahedral Zn–Zn separation distance is $\frac{1}{2}\langle 110 \rangle$. Such a Zn–Zn separation distance, however, automatically ensures that $\mathbf{u}_{O2'} = -\mathbf{u}_{O1'}$ so that $\mathbf{u}_{Bi} = 0$ and leads to a severely under-bonded Bi ion (AV of 2.320). It is therefore energetically extremely unfavourable and does not occur. This provides the crystal chemical rationale for why $\frac{1}{4}\langle 112 \rangle$ type Zn–Zn separation distances are strongly favoured and $\frac{1}{2}\langle 110 \rangle$ type Zn–Zn separation distances completely avoided in BZN-related pyrochlores.

The resultant picture described above is entirely compatible not only with the adp's of the O′ and A ions extracted from average structure refinements of BZN [6,8] but also with the distribution of atomic sites in the Monte Carlo simulation corresponding to the diffraction patterns shown in Figs. 3e and f (see Fig. 7 of [8]).

4.2. The local structure

Given the similarity of the observed and simulated EDPs (see Fig. 3), it is clear that the same local chemical ordering principles occur in both BZSN and BZTN as well as BZN itself i.e. all O′A_4 tetrahedra should have, as far as possible, stoichiometry O′Bi_3Zn while $\frac{1}{2}\langle 110 \rangle$ type inter-tetrahedral Zn–Zn separation distances should also be avoided. Applying these principles and assuming a 'marker' Zn ion at $\frac{1}{8}, \frac{1}{8}, \frac{1}{8}$ (marked by the open squares in Figs. 7a and b) there are two only Bi/Zn ordering patterns compatible with a P-centred resultant superstructure of average pyrochlore unit cell dimensions. The first, shown in Fig. 7a, has resultant $P4_332$ space group symmetry while the symmetry-related second, shown in Fig. 7b, has resultant $P4_132$ space group symmetry. The Zn ions are shown as large balls at the corners of the O′Bi_3Zn tetrahedra in Fig. 6 while the O′–Zn–O′ "zincanyl" type units are marked by the double-headed arrows. Note that the characteristic arrangement of

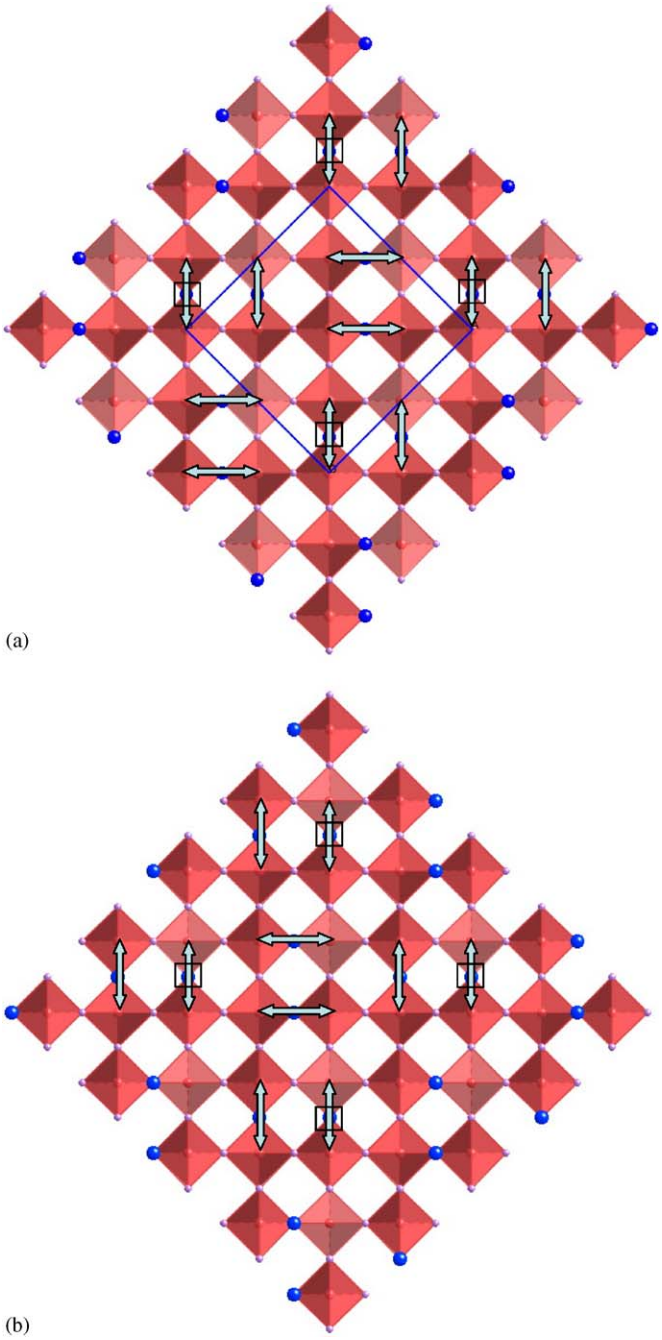

Fig. 7. Shows the two possible Bi/Zn ordering patterns compatible with a *P*-centred resultant superstructure of average pyrochlore unit cell dimensions in projection along an ⟨001⟩ direction. The projected pyrochlore type unit cell is shown outlined in (a). The two ordered distributions (assuming a 'marker' Zn ion at $\frac{1}{8}, \frac{1}{8}, \frac{1}{8}$) were obtained via the systematic application of the ordering principles that (i) all $O'A_4$ tetrahedra must have stoichiometry $O'Bi_3Zn$ and (ii) $\frac{1}{2}\langle 110\rangle$ type inter-tetrahedral Zn–Zn separation distances are not allowed. The first, shown in (a), has resultant $P4_332$ space group symmetry while the symmetry-related second, shown in (b), has resultant $P4_132$ space group symmetry. The Zn ions are shown as large balls at the corners of the $O'Bi_3Zn$ tetrahedra while the O′–Zn–O′ "zincanyl" type units are marked by the double-headed arrows.

Table 5
Proposed fractional co-ordinates of fully ordered $(Bi_{1.5}Zn_{0.5})(Ti_{1.5}Nb_{0.5})O_7$ (BZTN) in space group $P4_332$, $a = 10.3528$ Å

Atom	Wyckoff position	*x*	*y*	*z*	AV
Bi	12*d*	1/8	5/8 + 0.0238	5/8–0.0238	2.664
Zn	4*a*	1/8	1/8	1/8	2.001
Ti	12*d*	1/8	3/8	7/8	3.956
Nb	4*b*	5/8	5/8	5/8	5.127
O1	24*e*	−0.0548	3/4	3/4	1.660
O2	24*e*	−0.0548	1/4	1/4	2.144
O3	8*c*	0 + 0.0238	0 + 0.0238	0 + 0.0238	2.082

the O′–Zn–O′ "zincanyl" type units completely destroys the original face-centreing symmetry operations of the underlying pyrochlore type average structure. Relatively extended distributions of this type must occur in the case of BZNT in order to account for the sharpness of the observed "satellite reflections" (see e.g. Fig. 5).

Following the principles enunciated in the previous section and above, a fully ordered model structure for BZNT in space group $P4_332$, $a = 10.3528$ Å, has been derived. The proposed fractional co-ordinates and corresponding AVs are as given in Table 5. While the AV of the Bi and O1 ions remain somewhat under-bonded, the proposed structure is clearly chemically quite plausible, particularly given that the O1 and O2 ions are on general positions in space group symmetry $P4_332$ and are thus capable of relaxing to further fine tune the local crystal chemistry. Note that the only ions that have been allowed to relax away from their average structure positions in the proposed model structure are the O3 ions (corresponding to the O′ ions of the average structure) and the Bi ions. The O3 ions in this model have been allowed to displace along the appropriate ⟨111⟩ direction by 0.0238 ⟨111⟩ towards their neighbouring Zn ions while the induced Bi ion shifts are then along the appropriate 0.0238 ⟨011⟩ directions, etc.

The nearest neighbour Bi–Bi distances are then expanded by 4.73% from the average structure distance to 3.8464 Å while the nearest neighbour Bi–Zn distances are shrunk by 4.73% to 3.4991 Å. 'Size effect' like relaxations of this sort are known to cause intensity in diffuse distributions to be transferred either from the high angle to the low angle side of neighbouring average structure Bragg reflections or vice versa [8]. In our case, there is clear experimental evidence (see e.g. Fig. 5a) that the intensity in the 'satellite reflections' is transferred from the high to the low angle side of neighbouring average structure Bragg reflections (the satellite reflections on the low angle side of the parent $[\bar{8}80]^*$ pyrochlore Bragg reflection contained within the white box of Fig. 5a, for example, are noticeably more intense than those on the high angle side). In order to confirm this, Monte Carlo simulation (see [8] for details) was used to produce a 'size effect' relaxed $O'Bi_{1.5}Zn_{0.5}$ distribution starting with the undistorted $O'Bi_{1.5}Zn_{0.5}$

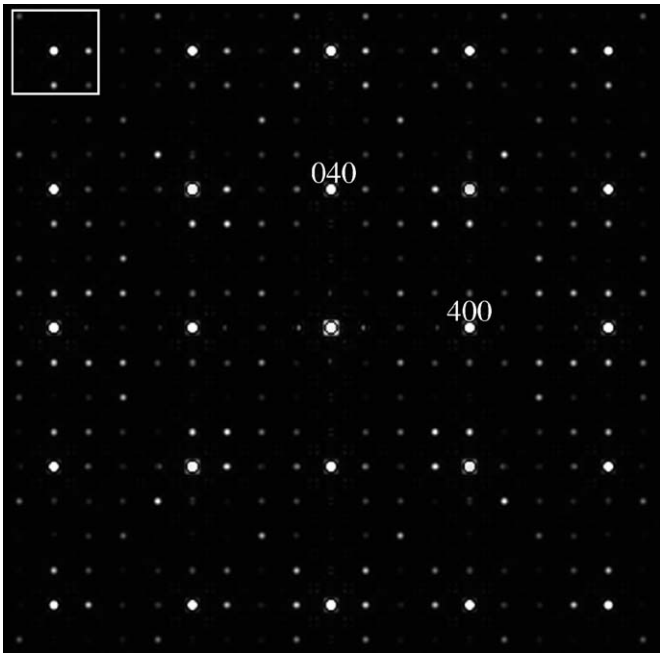

Fig. 8. An ⟨001⟩ diffraction pattern simulated using a 'size effect' relaxed $O'Bi_{1.5}Zn_{0.5}$ distribution starting with the undistorted $O'Bi_{1.5}Zn_{0.5}$ distribution of space group symmetry $P4_332$ shown in Fig. 7a.

distribution of space group symmetry $P4_332$ shown in Fig. 7a. Fig. 8 shows the corresponding simulated ⟨001⟩ type diffraction pattern using this distribution. Comparison with Fig. 5a shows good qualitative agreement (cf. e.g. the relative intensities of the satellite reflections around the $[\bar{8}\bar{8}0]^*$ pyrochlore Bragg reflection contained within the white box of Figs. 5a and 8) and confirms the plausibility of the proposed structural model.

5. Conclusions

The fundamental underlying crystal chemistry of BZN and BZN-related phases is based on strong local Bi/Zn ordering rules, namely each $O'A_4$ tetrahedra should have, as far as possible, the average $O'Bi_3Zn$ stoichiometry while $\frac{1}{2}\langle 110\rangle$ type inter-tetrahedral Zn–Zn separation distances should be completely avoided. The initial drastic underbonding of the Zn ions in the pyrochlore type average structure is overcome by the local formation of ZnO'_2 zincanyl type structural units involving the two apical O′ ions bonded to a central Zn ion contracting in strongly towards the central Zn ion. This in turn induces the neighbouring Bi ions to move off-centre towards two of the 6 surrounding equatorial O ions whilst simultaneously minimizing the separation distance to their two surrounding apical O′ ions (see Fig. 6).

Acknowledgments

YL and RLW acknowledge financial support from the Australian Research Council (ARC) in the form of an ARC Discovery Grant.

References

[1] H. Wang, D. Zhang, X. Wang, X. Yao, J. Mater. Res. 14 (1999) 546–548.
[2] X. Wang, H. Wang, X. Yao, J. Am. Ceram. Soc. 80 (1997) 2745–2748.
[3] M. Valant, P.K. Davies, J. Am. Ceram. Soc. 83 (2000) 147–153.
[4] J.C. Nino, M.T. Lanagan, C.A. Randall, J. Appl. Phys. 89 (2001) 4512–4516.
[5] S. Kamba, V. Porokhonsky, A. Pashkin, V. Bovtun, J. Petzelt, J.C. Nino, S. Trolier-McKinstry, M.T. Lanagan, C.A. Randall, Phys. Rev. B 66 (2002) 054106:1–8.
[6] I. Levin, T.G. Amos, J.C. Nino, T.A. Vanderah, C.A. Randall, M.T. Lanagan, J. Solid State Chem. 168 (2002) 69–75.
[7] J. Lu, S. Stemmer, Appl. Phys. Lett. 83 (2003) 2411–2413.
[8] R.L. Withers, T.R. Welberry, A.-K. Larsson, Y. Liu, L. Norén, H. Rundlöf, F.J. Brink, J. Solid State Chem. 177 (2004) 231–244.
[9] V.P. Sirotinkin, A.A. Bush, Inorg. Mater. 39 (2003) 974–977.
[10] A. Mergen, W.E. Lee, Mater. Res. Bull. 32 (1997) 175–189.
[11] C. Ang, Z. Yu, H.J. Youn, C.A. Randall, A.S. Bhalla, L.E. Cross, J. Nino, M. Lanagan, Appl. Phys. Lett. 80 (2002) 4807–4809.
[12] T. Vanderah, I. Levin, M. Lufaso, Eur. J. Inorg. Chem. (2005) 2895–2901.
[13] H. Du, X. Yao, L. Zhang, Ceram. Int. 28 (2002) 231–234.
[14] H. Du, X. Yao, Mater. Res. Bull. 40 (2005) 1527–1535.
[15] H. Du, X. Yao, J. Mater. Sci.: Mater. Electron. 15 (2004) 613–616.
[16] http://www.webelements.com/webelements/elements/text/periodic-table/bind.html
[17] N.E. Brese, M. O'Keeffe, Acta Crystallogr. B 47 (1991) 192–197.